Parity nonconservation in neutron resonances in ^{238}U

B. E. Crawford,[1,*] J. D. Bowman,[2] P. P. J. Delheij,[3] C. M. Frankle,[2] M. Iinuma,[4,†] J. N. Knudson,[2] L. Y. Lowie,[5,‡] A. Masaike,[4] Y. Matsuda,[4] G. E. Mitchell,[5] S. I. Penttilä,[2] H. Postma,[6] N. R. Roberson,[1] S. J. Seestrom,[2] E. I. Sharapov,[7] S. L. Stephenson,[5,§] Y.-F. Yen,[2,‖] and V. W. Yuan[2]

(TRIPLE Collaboration)

[1]*Duke University, Durham, North Carolina 27708*
and Triangle Universities Nuclear Laboratory, Durham, North Carolina 27708-0308
[2]*Los Alamos National Laboratory, Los Alamos, New Mexico 87545*
[3]*TRIUMF, Vancouver, British Columbia, Canada V6T 2A3*
[4]*Department of Physics, Kyoto University, Kyoto 606-8502, Japan*
[5]*North Carolina State University, Raleigh, North Carolina 27695-8202*
and Triangle Universities Nuclear Laboratory, Durham, North Carolina 27708-0308
[6]*University of Technology, Delft, 2600 GA, the Netherlands*
[7]*Joint Institute for Nuclear Research, 141980 Dubna, Russia*

(Received 6 April 1998)

Parity nonconservation (PNC) was studied for 24 *p*-wave neutron resonances in ^{238}U from 10 to 300 eV by measuring the helicity dependence of the total neutron cross section with an improved experimental apparatus. Six resonances show statistically significant (greater than 2.9σ) parity violation. An analysis treating the PNC matrix elements as random variables yields a root-mean-square PNC matrix element $M=0.67^{+0.24}_{-0.16}$ meV. The corresponding weak spreading width $\Gamma_w=(1.35^{+0.97}_{-0.64})\times10^{-7}$ eV. [S0556-2813(98)03708-X]

PACS number(s): 25.40.Ny, 24.80.+y, 11.30.Er, 27.90.+b

I. INTRODUCTION

The traditional view of symmetry breaking in the nucleus is exemplified by the approach to parity nonconservation (PNC) in light nuclei. Parity doublets (closely spaced, low-lying states of the same angular momentum and opposite parity) were studied. A parity-forbidden observable was measured and the wave functions for the initial and final states calculated with the shell model. After the discovery of a very large enhancement of parity violation for neutron resonances in heavy nuclei (as large as 10^6) [1], a new approach was adopted that considers the compound nucleus (CN) as a chaotic system and treats the symmetry breaking matrix elements as random variables. The experimental goal of the PNC experiments in the CN is the determination of the root-mean-square symmetry breaking matrix element. The CN is now considered as an excellent laboratory for the study of symmetry breaking. The difference in approach is illustrated by the differences between the classic review by Adelberger and Haxton [2] (where the PNC measurements in nucleon-nucleon scattering and the data from light nuclei are compared with the predictions of Desplanques, Donoghue, and Holstein [3]) and the recent reviews by Bowman *et al.* [4], Frankle *et al.* [5], and Flambaum and Gribakin [6].

In all of the early experiments only one PNC effect was measured per nuclide, due to the limited sensitivity and energy range studied. This is a crucial limitation, since a number of measurements are required for the statistical analysis. In our initial measurements the TRIPLE Collaboration measured a number of PNC effects in ^{238}U [7,8] and ^{232}Th [9,10]. Although the results were encouraging, the statistical quality of the initial data left much to be desired. In ^{238}U only one statistically significant effect was observed (there were several PNC effects at the 2σ level). Seven statistically significant PNC effects were observed in ^{232}Th. However, there was an unexpected nonstatistical result observed in ^{232}Th: all measured asymmetries have the same sign [9,10]. This result generated a large amount of interest and theoretical speculation—see the following paper on ^{232}Th [11]. It was therefore considered very important to repeat the measurements on uranium and thorium, improving both the quality of the data and the analysis. This paper and the following paper on ^{232}Th report the results of measurements and analysis following these improvements. The present measurement of ^{238}U shows six statistically significant PNC effects and gives a matrix element that is consistent with the previous result but has greater precision. In addition, the six PNC effects show both positive and negative signs, indicating that the sign effect seen in ^{232}Th is not a universal phenomenon. The ^{238}U data and analysis are reported in the dissertation of Crawford [12].

We define the PNC asymmetry p for an $l=1$ (p-wave) resonance from $\sigma_p^{\pm}=\sigma_p(1+p^{\pm})$, where $\sigma_p^{\pm}$ is the p-wave resonance cross section for $+$ and $-$ helicities, σ_p is the resonance part of the p-wave cross section, and the neutron polarization is assumed to be 1. The spirit of the analysis is

*Present address: North Carolina State University, Raleigh, NC 27695-8202 and Gettysburg College, Gettysburg, PA 17325.
†Present address: Hiroshima University, Hiroshima-Ken 739-8526, Japan.
‡Present address: McKinsey and Company, Atlanta, GA 30303.
§Present address: Gettysburg College, Gettysburg, PA 17325.
‖Present address: Wake Forest University School of Medicine, Winston-Salem, NC 27157.

that the resonance parameters are determined from the sum of the data from both helicity states (with a multilevel, multichannel code described below), and that these resonance parameters are then held fixed while the longitudinal asymmetries are determined separately for the + and − helicity states. Data for both helicity states obtained under similar conditions are summed in order to provide very good statistics. The neutron resonance parameters are determined from these summed data, including the resonance cross section σ_p for the p-wave resonance in question. The asymmetry parameters $p^{\pm}$ are determined from $\sigma_p^{\pm}$, and the PNC longitudinal asymmetry p is then determined from $p=(\sigma_p^+-\sigma_p^-)/(\sigma_p^+ +\sigma_p^-)=(p^+-p^-)/(2+p^++p^-)$.

The experimental system is described in Sec. II, with emphasis on the changes since the earlier measurements. Section III describes the procedure used to obtain the resonance parameters and the PNC longitudinal asymmetries. The data set is described in Sec. IV. The experimental results—resonance parameters and PNC longitudinal asymmetries—are presented in Sec. V. The analysis used to obtain the rms PNC matrix element from the asymmetries is discussed in Sec. VI.

II. EXPERIMENT

A. Polarized neutron beam facility

The intense pulsed epithermal neutron beam at the Manuel Lujan Neutron Scattering Center (MLNSC) is produced by 800-MeV proton pulses from the Los Alamos Neutron Science Center (LANSCE). The protons from the LANSCE linac are accumulated in a proton storage ring with typical average beam currents of ~60 μA and have the shape of an isosceles triangle with a base of 250 ns. After exiting the proton storage ring, the proton pulses interact with a tungsten spallation target at a rate of 20 Hz. Approximately 17 fast neutrons are produced for each incident proton. The neutrons are then moderated to epithermal energies in a water moderator and collimated. The neutron energy distribution has a Maxwellian shape with a tail that falls off approximately as $1/E$. The distribution peaks at about 40 meV. A detailed description of the target-moderator geometry is given by Lisowski *et al.* [13]. In addition to the initial pulse width that the neutrons acquire from the proton beam, further broadening is introduced by the moderation process. This additional contribution to the neutron beam resolution becomes important in fitting the line shape of the neutron resonances and is discussed in the next section.

Roberson *et al.* [14] discuss the experimental setup as utilized by the TRIPLE Collaboration in the original experiment on ^{238}U. Although we have since made major changes to the apparatus, the experimental philosophy is the same. Here we focus on the changes adopted since the earlier work. An overview of the polarized neutron beam facility is shown in Fig. 1.

As the neutron beam exits the spallation source, the flux is monitored by a pair of ionization chambers [15]. The first chamber is filled with ^{3}He gas and the second with ^{4}He gas. The first chamber is sensitive to neutrons via the $^3\mathrm{He}(n,p)^3\mathrm{H}$ reaction, while both chambers are sensitive to γ rays through the photoelectric effect and pair production.

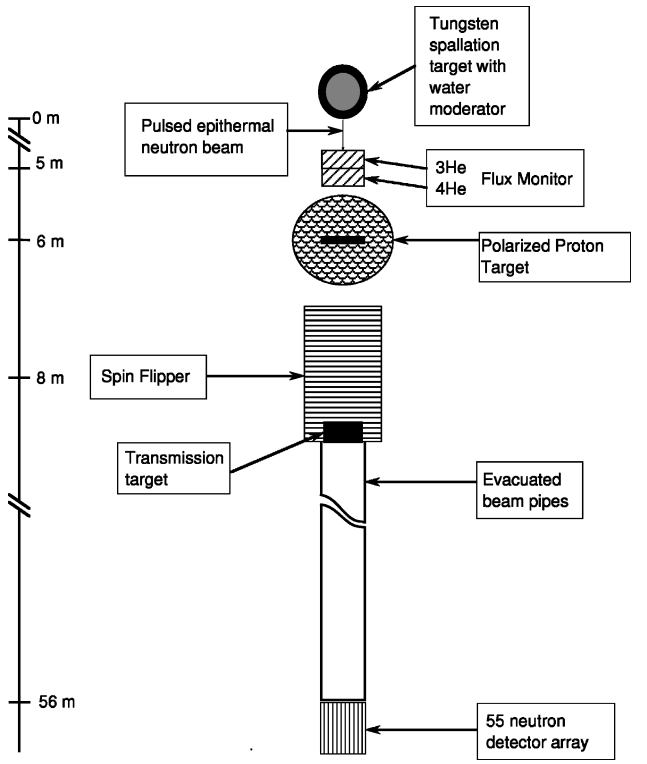

FIG. 1. Overview of polarized neutron flight path at LANSCE.

The difference between the counts in the two chambers yields the neutron flux. This monitor system is used not for an absolute measurement of the neutron flux, but rather as a sensitive (10^{-4} level) measure of the beam stability. In practice we reject neutron pulses for which the monitor counts (for a given time) vary beyond an accepted standard.

The neutron beam is polarized by transmission through a polarized proton target. The *n-p* elastic cross section has a strong spin dependence—the cross section for neutron and proton spins parallel (antiparallel) is 3.7 b (37.2 b)—and the cross section is constant over a large energy range, from 1 eV to several keV. The protons in ammonia are polarized by the dynamic nuclear polarization (DNP) method at 1 K in a 5-T magnetic field [16,17].

The DNP technique uses microwave pumping to populate the nuclear states of interest. With two different microwave transition frequencies one can obtain protons polarized parallel or antiparallel to the magnetic field direction, so that only the microwave frequency needs to be changed and not the magnetic field direction. Changing the proton-polarization direction provides a convenient way to check for possible systematic errors. However, since this change takes 1–2 h, it is performed only a few times during the 1–2 weeks it takes to study a typical target. The proton polarization is monitored with nuclear magnetic resonance (NMR). Since the NMR measurement does not probe the entire target volume equally, it may not provide a reliable absolute measurement. Instead it provides a rapid *relative* determination of the proton polarization. The NMR measurement can be calibrated by comparing the neutron transmission through the target while it is polarized and unpolarized, or by adopting the large PNC effect at 0.74 eV in ^{139}La as a standard and determining the neutron polarization from the measured

asymmetry. These methods are discussed in detail by Penttilä *et al.* [16] and Yuan *et al.* [18]. The typical neutron polarization was about 70%.

To reverse the spin direction of the neutrons rapidly, a ''spin flipper'' consisting of a series of longitudinal and transverse magnetic fields was designed and fabricated [19]. The longitudinal coils form a solenoidal field that points along the beam direction for the first half of the length of the spin flipper and opposite to the beam direction for the second half. The transverse field is produced by Helmholtz coils on both sides of the spin flipper and is perpendicular to the beam direction. As a function of distance along the beam direction, the longitudinal field follows a sine function, and the transverse field has a cosine dependence. Therefore, the addition of the two components produces a field with constant magnitude that rotates 180° over the length of the spin flipper.

With the transverse coils off, the neutrons pass through a magnetic field that reverses direction at the center of the spin flipper and which has very small transverse components. The neutrons of interest travel too fast to have their spins reversed. With the transverse coils on, the magnetic field rotates 180° over the length of the spin flipper. The neutrons adiabatically follow the magnetic field and emerge with their spins reversed. Effects of radial field components on off-axis neutrons and the energy dependence of the spin-flipping efficiency are discussed in detail by Bowman *et al.* [19].

At room temperature Doppler broadening is a significant effect; at 10 eV the Doppler width is roughly 3 times larger than the natural width of a typical ^{238}U p-wave resonance. To reduce this effect on the resonance line shape, the ^{238}U target was cooled to 77 K. The target was situated at the end of the spin flipper (approximately 9.7 m from the neutron source) such that the solenoidal magnetic field served as a guide field for the neutron spins as they interacted with the target.

The neutron detector system consists of a ^{10}B-loaded liquid scintillator ($C_{11}H_{10}+C_3H_9BO$) viewed by 55 photomultiplier tubes (PMT's) [20]. The scintillator is segmented into 55 cells arranged in a honeycomb pattern with each cell coupled to a PMT on the downstream side of the detector. The detector is located 57 m from the spallation source. The segmented nature of the detector allows very high instantaneous counting rates (as high as 500 MHz), while the thickness of the scintillator (4 cm) is such that most of the neutrons are thermalized and captured, giving the detector a very high and nearly energy-independent efficiency.

Since transmission experiments require a large amount (kilograms) of target material, they are often not feasible for isotopically pure samples. Therefore, an alternate detection system was developed. For p-wave neutron resonances in heavy nuclei the capture width is almost equal to the total width. Therefore, measuring the capture cross section is equivalent to measuring the total cross section. A capture γ-ray detector was designed and fabricated that consisted of 24 CsI detectors forming two annular rings that subtend a 3.3π solid angle. The initial design was discussed by Frankle *et al.* [21] and a description of the working system given by Crawford *et al.* [22]. For the capture experiment the target was located at 59 m, and solenoidal guide fields preserve the neutron polarization along the entire beam line [12]. In the present experiment the capture detector system was used only to determine the shape of the resolution function.

Two types of neutron absorbers were used in these experiments; both were located at the upstream end of the spin flipper. The purpose of the absorber is to remove low-energy neutrons from the beam in order to prevent them from reaching the detector after the next neutron pulse has occurred. The usual material is natural Cd, which has a large thermal cross section and a very large resonance at 0.178 eV. Unfortunately there is a resonance at 89.5 eV in ^{110}Cd that obscures the 89.2-eV resonance in ^{238}U. For this reason natural boron, which also has a large thermal cross section, was used as the absorber for about half of the uranium measurements.

B. Data acquisition

The data acquisition process is initiated with each proton burst. An inductive pickup on the proton beam line (before the spallation target) provides a time-zero signal t_0.

The detector signals are fed to discriminators and the outputs are linearly summed and filtered to 100, 200, or 1000 ns, where the filter time depends on the digital sampling interval (dwell time). (The choice of dwell time depends on what energy region of the time-of-flight spectrum is being studied. A 1-eV neutron takes $\sim$4 ms to reach the detector.) A transient recorder digitizes the summed detector signal 8192 times in intervals determined by the dwell time. The 8192 words are added to a summation memory for 200 beam bursts before being stored in computer memory. Since the neutron pulse rate is 20 Hz, there are 50 ms between pulses which permit a measurement of the background and electronic noise. One-sixtieth of a second after the initial t_0, a second electronic pulse t_0' is generated to initiate another sweep of the detector signal. The t_0' pulse also triggers the summation memory to subtract this second sweep from the stored data. In this way, the data from each neutron pulse are corrected for background and electronic noise. This correction is also applied to the monitor signal. The significance of 1/60 s is that most of the electronic noise is from 60 Hz pickup. This process is followed for 200 beam bursts, and then the 8192-channel spectrum is transferred to computer memory.

The state of the spin flipper is changed according to an eight-step sequence designed to reduce the effects of gain drifts and residual transverse magnetic fields on the PMT's [14]. The transverse field of the spin flipper is off or on according to the sequence $0++0-00-$, where 0 indicates that the transverse field is off and $\pm$ that the transverse field is on in the $\pm$ transverse direction. Each spin flipper state lasts 10 s (200 t_0 pulses). The data are stored in separate spectra, one for the NOFLIP state (0) and one for the FLIP state ($+$ or $-$). At the end of each eight-step sequence the beam-monitor data are averaged, and the entire eight-step sequence is considered ''bad'' if the flux from any beam burst deviates from the mean value by more than 8%. If the flux is stable, the data are considered ''good.'' Both data sets (good and bad) are stored (separately) in computer memory. After 20 eight-step sequences have been performed, the data collection is stopped and the data from this approximately 30-min collection period are stored as a ''run'' for later analysis. The result is a large number of small data sets, ''runs,'' during

which the experimental conditions should be sufficiently constant. These runs are analyzed separately.

III. DETERMINATION OF PNC LONGITUDINAL ASYMMETRIES

The fitting code FITXS [23] was developed specifically to fit the epithermal neutron time-of-flight spectra measured at LANSCE by the TRIPLE Collaboration. One chooses a particular time-of-flight (TOF) region and a set of fitting parameters, and then minimizes χ^2 to obtain the optimum set of values for these parameters. The fitting function depends on the target areal density n, the multilevel cross sections, and broadening due to three sources: the time structure of the neutron beam, the Doppler broadening due to the relative motion between neutrons and target nuclei, and the time response of the detector system. The broadening due to the beam and the detection system can be combined analytically to form a response function $B(t)$.

For this transmission experiment, the fitting function can be written as

$$\mathcal{F}_t(t)=B_t(t)\otimes[N_0(t)e^{-n\sigma_D(t)}]+\mathcal{B}, \tag{1}$$

where

$$\sigma_D(t)=[D(v)\otimes\sigma(v)]_{v\to t}, \tag{2}$$

N_0 is the neutron flux, $D(v)$ is the Doppler response function, $\mathcal{B}$ is the background function, and the $v\to t$ symbol indicates that after the convolution in velocity space, the function is converted to a function of time. The $\otimes$ symbol indicates a convolution.

Note that the convolutions in Eq. (1) do not commute. In order to extract correct resonance parameters and PNC asymmetries, the convolutions must be performed separately and in the proper order. The use of a generic fitting function that does not properly separate the effects of Doppler broadening from those of the beam and detection responses may yield incorrect asymmetries for strong resonances (large $n\sigma$) or for resonances where the intrinsic resonance width is small compared with the response width. This was one of the major problems with our earlier fitting program, in which all resolution effects were simulated by one effective Gaussian. The other major limitation in the earlier approach was the empirical determination of the off-resonance line shape. This tended to work well when a resonance was isolated and the nearby cross section smooth, but not for more complicated resonance structures.

The key element in the analysis is that the neutron cross section data are fit to determine the resonance parameters, which are then held fixed while the longitudinal asymmetries are determined for each run. The multilevel, multichannel neutron cross section is calculated with the formalism of Reich and Moore [24]. Since this formalism is widely used in the analysis of neutron resonances [25], using the same formalism and notation provides maximum consistency with the literature. For ^{238}U there is no fission and the ratio of the total resonance width Γ to the average level spacing D is small ($\Gamma/D\sim0.005$). However, the multilevel formalism is essential to reproduce level-level interference effects.

The s-wave elastic cross section for total angular momentum J is

$$\sigma^{\rm el}_{s:J}=\pi\lambda\!\!\!^{-2}g_J\left|1-e^{-2ikR}\left[1+\frac{2if_J}{1-if_J}\right]\right|^2, \tag{3}$$

with

$$f_J=\sum_{s:J}\frac{\Gamma^s_n/2}{E_s-E-i\Gamma^s_\gamma/2}, \tag{4}$$

where $g_J=(2J+1)/2$ is the statistical weighting factor for targets with spin $I=0$, $\lambda\!\!\!^{-}$ is the neutron wavelength divided by 2π, and R is the neutron channel radius. The experimentally determined potential scattering radius [26] is used for R. The resonance energy is $E_{s,p}$, the neutron width $\Gamma^{s,p}_n$, the γ-ray width $\Gamma^{s,p}_\gamma$, and the total width $\Gamma^{s,p}$, all for s- and p-wave resonances, respectively.

The s-wave capture cross section is

$$\sigma^{\gamma}_{s:J}=4\pi\lambda\!\!\!^{-2}g_J\frac{{\rm Im}\{f_J\}}{[1+{\rm Im}\{f_J\}]^2+{\rm Re}\{f_J\}^2}. \tag{5}$$

With $\Gamma_n\ll\Gamma_\gamma\ll D$, and the p-wave hard sphere phase shift neglected [27], the p-wave elastic cross section is

$$\sigma^{\rm el}_{p:J}=\pi\lambda\!\!\!^{-2}g_J\sum_{p:J}\frac{\Gamma^p_n\Gamma^p_n}{(E_p-E)^2+(\Gamma^p)^2/4}. \tag{6}$$

Similar simplifications can be used for the p-wave capture cross section [24], yielding

$$\sigma^{\gamma}_{p:J}=\pi\lambda\!\!\!^{-2}g_J\sum_{p:J}\frac{\Gamma^p_n\Gamma^p_\gamma}{(E_p-E)^2+(\Gamma^p)^2/4}. \tag{7}$$

The neutron widths are calculated at energy E according to

$$\Gamma^{s,p}_n(E)=\Gamma^{s,p}_n(E_{s,p})[E/E_{s,p}]^{l+1/2}. \tag{8}$$

The total cross section for both s- and p-wave resonances is simply the sum of the elastic and capture cross sections.

Initial investigations into the resolution function were performed by Yen *et al.* [28]. They obtained fits to Monte Carlo simulations of the beam time response for the TRIPLE beam line by convoluting a Gaussian with offset t' and width η, with an exponential with characteristic decay time τ:

$$\begin{aligned}M(t)&=\frac{1}{\sqrt{2\pi\eta^2}}\exp\left[-\frac{(t-t')^2}{2\eta^2}\right]\\&\quad\otimes\frac{1}{\tau}\exp\left[\frac{-(t-t')}{\tau}\right]u(t-t')\\&=\frac{1}{2\tau}\exp\left[\frac{-(t-t')}{\tau}+\frac{\eta^2}{2\tau^2}\right][1-{\rm erf}(Z)],\end{aligned} \tag{9}$$

where $u(t)$ is a unit step function, and $Z=[\eta/\tau-(t-t')/\eta]/\sqrt{2}$. In the energy range 1–1000 eV the three parameters were found to be given by $t'=2.79E^{-0.48}$ μs, $\eta=0.65E^{-0.51}$ μs, and $\tau=0.99E^{-0.37}$ μs.-

There are two more sources of broadening that are common to both the CsI capture detector and the transmission system: the proton beam shape from the proton storage ring and the electronic shaping before the transient digitizer. These can be approximated by Gaussian functions and convoluted with the Gaussian function from the beam response. The width of the resulting Gaussian is $\kappa^2=\eta^2+\sigma_{\rm PSR}^2+\sigma_{\rm elec}^2$.

For neutron resonances above 400 eV most of the observed width is from the neutron beam. A number of resonances were studied with the capture detector in order to determine the actual beam response in detail. Since we had studied parity violation via the capture reaction with small isotopic samples of ^{106}Pd and ^{108}Pd [12], we used these data to determine the beam response function. The fits at these energies were not especially sensitive to the Gaussian width, but were quite sensitive to the exponential tail. Initial fits to the ^{106}Pd and ^{108}Pd capture data with Eq. (9) were inadequate because of a long, low-energy (high-TOF) tail. We adopted a functional form found by convoluting the above expression with a second exponential with characteristic decay time τ_2:

$$B_c(t)=\frac{1}{2\tau}\exp\left[\frac{-(t-t')}{\tau}+\frac{\kappa^2}{2\tau^2}\right][1-\mathrm{erf}(Z)]+\frac{\epsilon}{2\tau_2}\exp\left[\frac{-(t-t')}{\tau_2}+\frac{\kappa^2}{2\tau_2^2}\right][1-\mathrm{erf}(Z_2)], \tag{10}$$

where $Z_2=[\kappa/\tau_2-(t-t')/\kappa]/\sqrt{2}$. From fitting resonances in ^{106}Pd and ^{108}Pd, we found $\epsilon=0.20$ and $\tau_2=3.9E^{-0.38}$ μs.

The transmission data showed an additional broadening from the neutron detector. The moderation process in the hydrogen-containing liquid scintillation detector is given by an exponential with characteristic decay time τ_d. The final result for the response function is

$$B_t(t)=\frac{1}{2(\tau-\tau_d)}\{e^{-(t-t')/\tau_d+\kappa^2/2\tau_d^2}[1-\mathrm{erf}(Z_d)]-e^{-(t-t')/\tau+\kappa^2/2\tau^2}[1-\mathrm{erf}(Z)]\}+\frac{\epsilon}{2(\tau_2-\tau_d)}\{e^{-(t-t')/\tau_d+\kappa^2/2\tau_d^2}[1-\mathrm{erf}(Z_d)]-e^{-(t-t')/\tau_2+\kappa^2/2\tau_2^2}[1-\mathrm{erf}(Z_2)]\}, \tag{11}$$

where $Z=[\kappa/\tau-(t-t')/\kappa]/\sqrt{2}$, $Z_d=[\kappa/\tau_d-(t-t')/\kappa]/\sqrt{2}$, and $Z_2=[\kappa/\tau_2-(t-t')/\kappa]/\sqrt{2}$. The average value of $\tau_d=416$ ns was determined from fitting nine resonances in ^{108}Pd. The details are given by Crawford [12].

Including an energy-dependent flux and a background function (described by a polynomial in time), the final fitting function can be written as

$$\mathcal{F}_t(t)=\left[B_t(t)\otimes\left(\frac{\alpha}{E^\beta}e^{-n\sigma_D(t)}\right)\right]+\sum_{i=1}^{3}\frac{a_i}{t^i}, \tag{12}$$

where $\sigma_D(t)$ is the Doppler-broadened total cross section for *s*- and *p*-wave resonances. The *s*- and *p*-wave cross sections are calculated for all resonances present (including contaminants) and summed to form the total elastic and capture cross sections.

When final satisfactory fits are obtained for all energy regions, all of the resonance parameters are considered known and are held fixed in subsequent analyses. At this point fits are obtained in each energy region for each helicity state for every run, varying only the longitudinal asymmetry. As described in the Introduction, once the cross sections $\sigma_p^{\pm}$ are determined, the PNC longitudinal asymmetries are easily obtained. A detailed description of the code FITXS is given by Matsuda [23].

IV. DATA

The ^{238}U target was a cylinder 6.32 cm long and 9.79 cm in diameter that was depleted of ^{235}U. For a density of 18.9 g/cm^3, this corresponds to an areal density of 3.025×10^{23} atoms/cm^2. From fitting known resonances in ^{235}U, the amount of ^{235}U contamination was determined to be $(0.21\pm0.01)\%$.

The ^{238}U experiment was run in transmission with the apparatus described in Sec. II. Preliminary examination of the data consisted of numerous checks for possible difficulties, such as fluctuations in peak height for selected resonances (indicating unstable timing) or a large number of ''bad'' spectra (indicating significant beam variation). All of the runs were also checked for asymmetric flux, which would lead to false asymmetries. This check was performed by calculating the ratio of the counts in the NOFLIP to the FLIP spectra for selected regions throughout the time-of-flight spectrum. No flux asymmetries were observed. After these checks, there were 157 good runs from which to determine the PNC effects in ^{238}U.

The initial energy calibration was performed using the energies of known resonances in ^{235}U and ^{238}U. This initial calibration was then used with the fitting code FITXS described in Sec. III and known resonances to fit the spectrum while varying the beam line length and the time-of-flight offset. The resulting values were beam length $L=56.736$ m and channel offset $C_0=2.71$ channels.

The statistical uncertainty in these values is very small, but the total error is undetermined since the uncertainties in the ENDF/B-VI [29] energies are unknown. Our data were also compared with the results of a measurement at ORELA [30] and appear to agree better with the ORELA values. By using the above energy calibration, the resonance energies were converted to time-of-flight channels and related to the ORELA resonance energies by $E=1.308\times10^5L^2/(C+C_0)^2$. Including the uncertainty in the energies from the ORELA experiment, a least squares fit was used to determine a new length $L=56.739\pm0.002$ m and a new channel offset $C_0=2.85\pm0.05$ channels. From this calibration the resonance energies and their uncertainties were determined. Differences between the energies extracted from the Cd- and B-absorber data were included in the uncertainty (these differences were noticeable primarily for the low-energy *s*-wave resonances). Our values have smaller uncertainties for

TABLE I. Resonance parameters for ^{238}U.

E (eV)	BP[a]	l	J[b]	$g\Gamma_n$ (meV)	Γ_γ (meV)	A_i (1/eV)
10.2349±0.0007	0.99	1	1.5	0.001 68±0.000 05		
11.3089±0.0008	1.00	1	0.5	0.000 41±0.000 01		46.9
19.521±0.001	0.99	1	1.5	0.001 50±0.000 05		
20.866±0.006	0.00	0	0.5	10.6±0.3	21.1±0.8	
36.67±0.02	0.00	0	0.5	34.8±1.1	20.3±0.9	
45.158±0.004	0.99	1	0.5	0.002 05±0.000 07		35.7
49.613±0.004	0.99	1		0.001 08±0.000 02		37.7
63.496±0.005	0.99	1	0.5	0.0094±0.0003		41.1
66.02±0.02	0.00	0	0.5	24.7±0.9	21.9±0.9	
72.373±0.006	0.99	1		0.0018±0.0002		42.3
80.741±0.007	0.00	0	0.5	1.7±0.2	26.8±3.7	
83.672±0.007	0.99	1	0.5	0.0090±0.0003		15.6
89.218±0.008	0.84	1	0.5	0.085±0.003		5.03
93.081±0.008	0.99	1	1.5	0.0062±0.0002		
97.975±0.009	0.99	1	1.5	0.0044±0.0002		
102.60±0.08	0.00	0	0.5	71.7±2.2	23.8±1.0	
111.18±0.01	0.99	1		0.0067±0.0005		33.1
116.89±0.02	0.00	0	0.5	25.3±1.0	23.3±1.3	
124.94±0.01	0.99	1	1.5	0.0196±0.0007		
133.18±0.01	0.99	1		0.0078±0.0003		12.0
145.64±0.02	0.00	0	0.5	0.74±0.02	26.9±1.0	
152.39±0.02	0.98	1	1.5	0.052±0.002		
158.94±0.02	0.99	1	1.5	0.0164±0.0005		
165.26±0.03	0.00	0	0.5	3.2±0.2	22.9±2.2	
173.18±0.02	0.98	1	0.5	0.048±0.002		7.96
189.70±0.06	0.00	0	0.5	174.2±5.2	29.6±2.0	
208.47±0.02	0.00	0	0.5	51.0±1.7	23.8±1.7	
214.85±0.02	0.98	1		0.055±0.002		10.9
218.33±0.02	0.98	1		0.036±0.004		9.85
237.34±0.05	0.00	0	0.5	25.8±0.9	23.4±1.3	
242.67±0.03	0.93	1	0.5	0.203±0.009		4.63
253.84±0.03	0.97	1	1.5	0.116±0.004		
257.17±0.03	0.98	1		0.025±0.002		6.58
263.89±0.03	0.92	1	1.5	0.259±0.008		
273.61±0.04	0.00	0	0.5	24.3±0.7	24.6±1.0	
282.41±0.03	0.97	1	1.5	0.112±0.004		
290.96±0.04	0.00	0	0.5	16.1±0.5	23.3±1.0	

[a]Bayesian *p*-wave probability.

[b]J values for *p*-wave resonances from Gunsing *et al.* (Ref. [42]).

the small *p*-wave resonances than the ORELA experiment due to the higher statistics of the present measurement. All resonance energies agree with the ORELA results within error. The energies and their uncertainties are listed in Table I. It should be noted that not all of the resonances in the ENDF/B-VI and ORELA tabulations were seen in the present measurements due to finite energy resolution and the effect of very strong and broad *s*-wave resonances, which is the result of using a thick target optimized for the study of parity nonconservation, not resonance analysis.

As the next step in the data analysis the transmission spectra were corrected for electronic and detector dead times [12] and for the γ-ray background in the neutron beam [31]. At this stage the data are ready for analysis with the fitting program FITXS.

V. DATA REDUCTION

A. Neutron resonance parameters

To determine the resonance parameters, ten runs were summed as a compromise between obtaining very good statistics and maintaining uniform experimental conditions. Since the cadmium and boron absorbers affected the shape of the flux differently (especially in the low-energy region), data from the two absorbers were analyzed separately. The ^{238}U target was sufficiently thick that many of the *s*-wave resonances absorbed all of the neutrons (such resonances are said to be ''black'' resonances). After the standard background correction [31] was applied, there were still some counts under the black resonances. The background parameters used in the program FITXS were determined by fitting

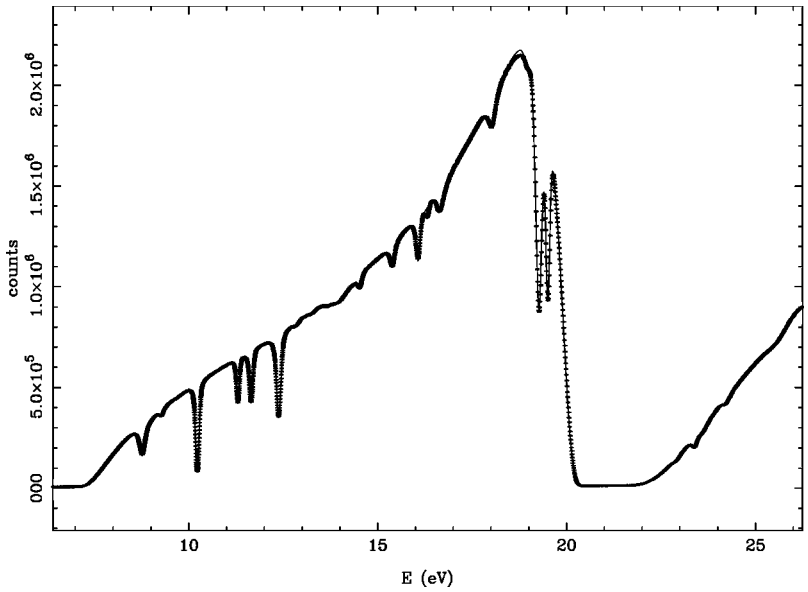

FIG. 2. Sample multilevel fit to the ^{238}U transmission spectrum in the energy region 6–26 eV. The data are from a sum of both helicity states for 10 half-hour runs. The very large dips are from the *s*-wave resonances at 6.6720 eV and 20.866 eV. In addition to the ^{238}U *p*-wave resonances at 10.2349 eV, 11.3089 eV, and 19.521 eV, there are many ^{235}U *s*-wave resonances visible in the figure, such as the resonances at 11.67 eV, 12.40 eV, and 19.29 eV.

these remaining counts to a polynomial function of 1/TOF. These parameters were then held fixed for the remainder of the fitting process.

The many large *s*-wave resonances dominate the spectrum. The procedure was first to fit a large energy region with known *s*-wave parameters and to allow the flux and its energy dependence to vary. The energy dependence was determined to be $E^{-0.948}$ and was then held constant. Then, a smaller energy region with a few *s*-wave resonances was fit, allowing E_s, $g\Gamma_n^s$, and Γ_γ^s to vary. Then, this process was repeated while including a higher-energy region with a few additional *s*-wave resonances. The initial resonance parameters were held fixed, and the parameters for the new resonances varied. The process was then repeated until all of the *s*-wave parameters were stable. Then, the *p*-wave resonances in isolated regions were fit, while allowing only the flux and the *p*-wave resonance parameters to vary. The flux showed a 2% fluctuation which contributes to the resonance width uncertainties. This analysis was performed on the data from the experiments with the Cd absorber and the B absorber. The resulting fits were normally very good, as illustrated by a sample fit shown in Fig. 2.

The final values for the resonance parameters are given in Table I. The errors on $g\Gamma_n$ and Γ_γ include statistical uncertainty, the error from averaging results from the Cd-absorber data and the B-absorber data, and an additional 3% uncertainty from the fitting process. This final 3% is an attempt to include systematic uncertainties from the fitting process and the effect of uncertainty in the response parameters. However, since this analysis relies heavily on the ^{238}U resonance data of ENDF/B-VI and ORELA, there is the possibility that systematic errors in those data are present in the current results. In that sense, the present determinations of the resonance parameters (energies and widths) cannot be viewed as completely independent of the ORELA results and ENDF/B-VI evaluation, but rather as an increase in the precision of the previous results. In general our results agree with the previous results except for many of the small *p*-wave resonances, where the present measurement has much higher statistics.

Since the measurement determines the value of $g\Gamma_n$, and not the value of the orbital angular momentum l, there is the possibility of ambiguity between a strong *p*-wave resonance and a weak *s*-wave resonance. We used the Bayesian analysis procedure of Bollinger and Thomas [32] to determine (in a probabilistic sense) the orbital angular momentum of each resonance. The Bayesian analysis uses the measured widths together with strength functions and level densities. The key to the method is simply that due to the large difference in penetrabilities, most of the small resonances are *p*-wave and most of the large resonances are *s*-wave. The probability of being a *p*-wave resonance can be written as

$$P(p,g\Gamma_n)=\left\{1+\frac{\pi_s}{\pi_p}\sqrt{3\frac{\pi_s}{\pi_p}\frac{S_1C_0(E)}{S_0C_1(E)}}\times\exp\left[\frac{-g\Gamma_n}{2}\frac{C_0(E)}{D_0}\times\left(\frac{1}{S_0}-\frac{\pi_p}{3\pi_s}\frac{C_1(E)}{C_0(E)S_1}\right)\right]\right\}^{-1}, \tag{13}$$

where π_s and π_p are the *a priori* probabilities of forming an *s*- or *p*-wave resonance, D_0 is the *s*-wave level spacing, S_0 and S_1 are the *s*- and *p*-wave strength functions, and

$$C_l(E)=\frac{1+(kR)^l}{(kR)^{2l}\sqrt{E(eV)}}. \tag{14}$$

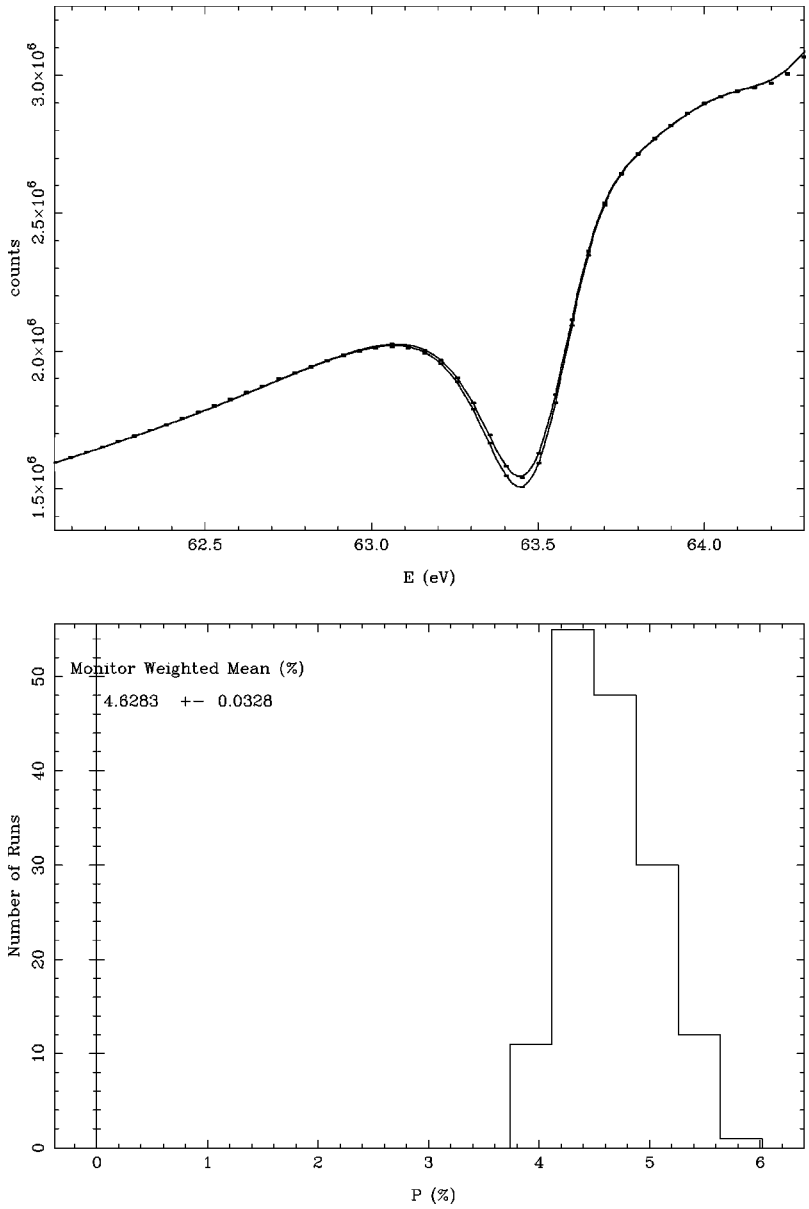

FIG. 3. Top: ^{238}U transmission spectra for two helicity states near the 63.4-eV resonance. The parity violation is apparent by inspection. Bottom: histogram of the asymmetries obtained for each of 157 runs for the resonance shown at the top of the figure.

The strength functions are given by

$$S_l = \frac{1}{2l+1} \frac{\langle g\Gamma_n^l \rangle}{D_l}, \tag{15}$$

where $g\Gamma_n^l$ is the reduced neutron width given by

$$g\Gamma_n^l = C_l(E) g\Gamma_n . \tag{16}$$

Mughabghab *et al.* [33] give $D_0 = (20.9 \pm 1.1)$ eV, $S_0 = (1.2 \pm 0.1) \times 10^{-4}$, $S_1 = (1.7 \pm 0.3) \times 10^{-4}$, and $R = 9.6$ fm. From our data we determined the values for the spacing and the strength functions to be $D_0 = (21 \pm 3)$ eV, $S_0 = (1.6 \pm 0.6) \times 10^{-4}$, and $S_1 = (1.2 \pm 0.4) \times 10^{-4}$, all of which agree with the values given by Mughabghab *et al.* We used the values from Mughabghab *et al.* in determining the Bayesian probability from Eq. (13) (see Table I). Our results for l agree very well with the ENDF/B-VI assignments except for the 257.22-eV resonance, for which our analysis yields a probability of 0.98 of having $l = 1$, as opposed to the quoted value of $l = 0$.

B. PNC longitudinal asymmetries

The asymmetries were obtained by using the code FITXS to fit each run, varying the asymmetry parameter while holding all other parameters constant. First, the sum of the two helicity states (NOFLIP+FLIP) was fit to determine the flux for a single run. Then, with all parameters held fixed except the asymmetry parameter, the data for each helicity state were fit separately to determine p^+ and p^- for each run. The asymmetry p is then determined. The neutron polarization was determined for each run and the correction made. (The observed asymmetry is the product of the neutron polarization times the true asymmetry.) The asymmetries for a sample resonance are shown in Fig. 3. The average p values and

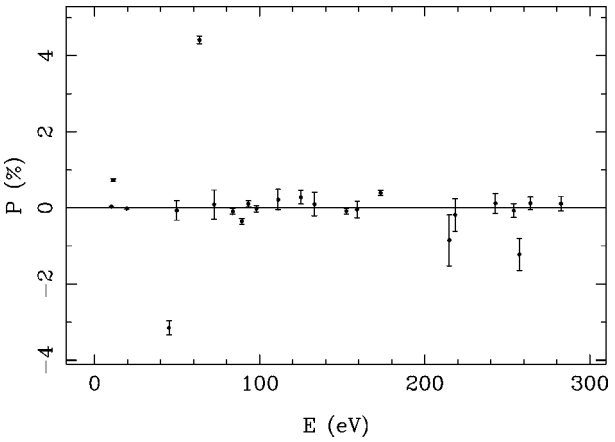

FIG. 4. Longitudinal asymmetries p versus energy E for ^{238}U.

their uncertainties were determined separately for each absorber and for each polarization orientation. These four values were then combined to yield the final observed value of the PNC longitudinal asymmetry for each resonance. The asymmetry values for all resonances were then corrected for the spin-flipping efficiency, which is a function only of neutron energy. These final asymmetry values are shown as a function of energy in Fig. 4 and are listed in Table II.

Significant information can be obtained directly from the PNC longitudinal asymmetries. For example, the average value of p is 0.1 ± 0.9 % (0.02 ± 0.24 %) when only effects with greater than 2σ statistical significance are considered (all effects are considered). This is consistent with the value of zero expected when the signs are random.

The general form for the magnitude of the longitudinal asymmetry implies an energy dependence of $E^{-1/2}$. The product $p\sqrt{E}$ is also included in Table II.

The magnitude of the difference in cross sections for the two helicity states is also of interest and has been explicitly considered by Carlson *et al.* [34]. For the ^{238}U data the average value

$$\overline{\Delta\sigma}=\overline{(\sigma_+-\sigma_-)}=\overline{2p(2.608\times10^6/E)(g\Gamma_n/\Gamma)}=65\pm86\ \text{mb}$$

for greater than 2σ effects and 20 ± 79 mb for all effects. The uncertainties are dominated by the distribution of $\Delta\sigma$ values rather than the measurement precision. Therefore, the above averages were not weighted by the measurement uncertainty. Again the average value is consistent with zero, as expected for random signs.

VI. ANALYSIS

A. Method

For a target with $I^\pi=0^+$, the s-wave resonances have $1/2^+$ and the p-wave resonances $1/2^-$ or $3/2^-$. Only $1/2^-$ resonances mix with the $1/2^+$ resonances to show parity violation. The two-level approximation has been obtained by many authors [35–39]. The observed PNC asymmetry p_μ for p-wave resonance μ is due to an admixture from a number of s-wave resonances ν [7],

$$p_\mu=2\sum_\nu \frac{U_{\nu\mu}}{E_\nu-E_\mu}\frac{g_{\nu_{1/2}}g_{\mu_{1/2}}}{\Gamma_n^\mu}, \tag{17}$$

TABLE II. PNC asymmetries for ^{238}U.

E (eV)	p (%)	$p/\Delta p$	$p\sqrt{E}(\%\sqrt{\text{eV}})$
10.2349	0.034 ± 0.016	2.1	0.11
11.3089	0.728 ± 0.038	19.3	2.45
19.521	-0.016 ± 0.018	−0.9	−0.07
45.158	-3.15 ± 0.18	−17.1	−21.2
49.613	-0.066 ± 0.26	−0.3	−0.46
63.496	4.41 ± 0.10	44.9	35.1
72.373	0.09 ± 0.38	0.2	0.77
83.672	-0.090 ± 0.079	−1.1	−0.82
89.218	-0.351 ± 0.078	−4.5	−3.32
93.081	0.108 ± 0.080	1.4	1.04
97.975	-0.024 ± 0.081	−0.3	−0.24
111.18	0.22 ± 0.27	0.8	2.32
124.94	0.28 ± 0.18	1.5	3.13
133.18	0.10 ± 0.31	0.3	1.15
152.39	-0.085 ± 0.080	−1.1	−1.05
158.94	-0.04 ± 0.22	−0.2	−0.50
173.18	0.398 ± 0.064	6.3	5.24
214.85	-0.85 ± 0.67	−1.3	−12.5
218.32	-0.18 ± 0.43	−0.4	−2.66
242.67	0.12 ± 0.26	0.4	1.87
253.84	-0.07 ± 0.18	−0.4	−1.12
257.17	-1.22 ± 0.42	−2.9	−19.6
263.89	0.12 ± 0.17	0.7	1.95
282.41	0.11 ± 0.19	0.6	1.85

where $g_{\mu_{1/2}}$ and $g_{\nu_{1/2}}$ are the neutron decay amplitudes of levels μ and ν ($g_\mu^2=\Gamma_n^\mu$ and $g_\nu^2=\Gamma_n^\nu$), and $U_{\nu\mu}$ is the matrix element of the PNC interaction between levels ν and μ. According to the statistical model of the compound nucleus, the signed quantities $U_{\nu\mu}$, g_μ, and g_ν are statistically independent random variables with mean-zero Gaussian distributions. One cannot obtain the individual matrix elements—there are too few equations and too many unknowns. However, one can determine the *variance* of the distribution of these matrix elements. The common variance M^2 of the PNC matrix elements is the mean-square matrix element of the PNC interaction.

The quantity p_μ is the sum of Gaussian random variables and therefore is itself a Gaussian random variable. The variance of p_μ is $M^2A_\mu^2$, where

$$A_\mu^2=\sum_\nu A_{\nu\mu}^2 \quad\text{and}\quad A_{\nu\mu}^2=\left(\frac{2}{E_\nu-E_\mu}\right)^2\frac{\Gamma_n^\nu}{\Gamma_n^\mu}. \tag{18}$$

Since there are only a limited number of data points for each nuclide, a maximum likelihood approach to the analysis seems suitable [40,41]. The probability density function (PDF) of the PNC asymmetry p_μ is a Gaussian $G(p_\mu,M^2A_\mu^2)$ with mean zero and variance $M^2A_\mu^2$. Including the experimental error σ_μ yields a Gaussian PDF with variance $M^2A_\mu^2+\sigma_\mu^2$:

$$G(p,M^2A_\mu^2+\sigma_\mu^2). \tag{19}$$

If all spectroscopic information is known, then the likelihood function for a given p-wave resonance μ is

$$L(M)=G(p_\mu,M^2A_\mu^2+\sigma_\mu^2)P_M(M), \tag{20}$$

where P_M is the *a priori* probability density, p_μ is the experimental value of the PNC asymmetry, and σ_μ is the uncertainty in p_μ. In order to obtain a normalizable function the simplest assumption is that the prior P_M is constant from $M=0$ to $M_{\max}$ and zero above $M_{\max}$. For a number of independent resonances the likelihood function is the product of the functions for the individual resonances. One inserts the values of the experimental asymmetries p_μ and their uncertainties σ_μ, determines the spectroscopic terms A_μ from the known resonance parameters, and calculates the likelihood function. The location of the maximum gives the most likely value m_L of the parameter M. The choice of a confidence interval for an asymmetric distribution is the subject of appreciable discussion. In practice it is usually sufficient to solve the equation

$$\ln\left[\frac{L(m_\pm)}{L(m_L)}\right]=\frac{1}{2}, \tag{21}$$

where $m_\pm$ are the corresponding upper and lower values at which this equation is satisfied.

If the p-wave spins are not known, then we consider the likelihood function as the sum of two terms. One term is as before [Eq. (20)], and one term is a Gaussian containing only the experimental error,

$$L(M)=[a(1/2)G(p_\mu,M^2A_\mu^2+\sigma_\mu^2) + b(3/2)G(p_\mu,\sigma_\mu^2)]P_M(M), \tag{22}$$

where a and b are the probabilities that $J=1/2$ or 3/2. (Since the $p_{1/2}$ and $p_{3/2}$ states have different average strengths, and there is a finite threshold for observability, the number of resonances actually observed does not have the expected statistical ratio. The relative probability is determined empirically from the data.) The *a priori* probability P_M is common to both terms. Note that since the second term is independent of M, the function is not normalizable without the factor P_M. In practice we assume that P_M is constant up to some maximum value and zero above this value. The justification for this form of the likelihood function is discussed in general by Bowman *et al.* [40] and in detail by Bowman, Lowie, and Sharapov [41].

This discussion assumes that all spectroscopic information is known. This is not true in general, and especially when the target spin is nonzero. We have developed an analysis approach suitable for targets with nonzero spin [40]. Our philosophy is to permit inclusion of partial information, since one almost always has some information but rarely all of the relevant spectroscopic information. Although the analysis becomes much more complicated, it can always be performed by inclusion of the available spectroscopic information (and averaging over the unknown parameters). The price of averaging is to increase the uncertainty in the value of M.

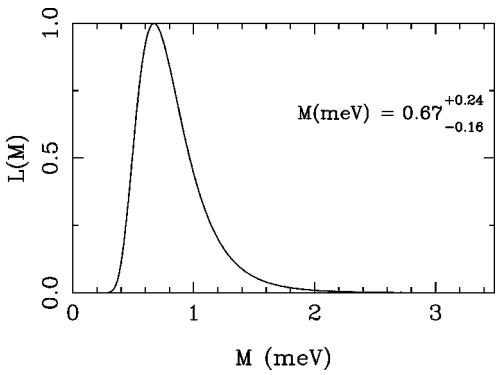

FIG. 5. Maximum likelihood plot for ^{238}U.

B. Results for the rms matrix element

The approach described above treats the lack of knowledge concerning the spins in a straightforward fashion. However, for ^{238}U the spins of most of the p-wave resonances studied in this paper have been measured by Gunsing *et al.* [42] via neutron capture measurements (see Table I). This provides an opportunity to test the validity of the assumed form for the likelihood function [Eq. (22)]. First, we included the seven known $p_{1/2}$ resonances, excluded the seven known $p_{3/2}$ resonances, and treated the remaining seven resonances as unknown, following the prescription of Eq. (22). The resulting maximum likelihood plot for ^{238}U is shown in Fig. 5. Then, the analysis was repeated, assuming that all of the resonances have unknown spins. The relative probabilities for observing $p_{1/2}$ and $p_{3/2}$, a and b, respectively, were determined to be $a=0.39$ and $b=0.61$ by following the procedure described by Frankle *et al.* [10].

The value for the rms PNC matrix element is $M=0.67^{+0.24}_{-0.16}$ meV for the first case (using the maximum information) and $M=0.69^{+0.26}_{-0.17}$ meV for the second case (all resonances treated as unknowns). Both of these values agree with our previous result $M=0.56^{+0.41}_{-0.20}$ meV [8]. There is very little difference when the maximum available information is used or when the purely statistical approach is adopted. The physical reason for this is that resonances that show no statistically significant parity violation (whether $p_{3/2}$ states that *cannot* display parity violation or $p_{1/2}$ states that *accidentally* have only a small parity violation) have very little effect on the final value of M. From the value of M and ΔM obtained using the first method, the value of the spreading width $\Gamma_w=2\pi M^2/D=(1.35^{+0.97}_{-0.64})\times10^{-7}$ eV.

VII. SUMMARY

PNC longitudinal asymmetries have been measured for 24 p-wave resonances in ^{238}U with an improved experimental system. Six p-wave resonances show parity violation with greater than 2.9σ statistical significance. These new results demonstrate a dramatic improvement in the data quality relative to our earlier measurement, which showed only one statistically significant PNC effect. The data are consistent with the expectation that only p-wave resonances with the proper angular momentum value show parity violation. A method of determining the longitudinal asymmetry has been developed that properly incorporates the several resolution convolutions, as well as correctly describing the multilevel, multi-

channel cross sections. The value of the rms PNC matrix element $M=0.67^{+0.24}_{-0.16}$ meV, which agrees with the earlier result. Since the spins of most of the *p*-wave resonances have been measured in a separate experiment, these data also confirm the Bayesian analysis adopted by TRIPLE. With an average level spacing of $D=20.9$ eV, the weak spreading width $\Gamma_w=(1.35^{+0.97}_{-0.64})\times10^{-7}$ eV.

ACKNOWLEDGMENTS

This work was supported in part by the U.S. Department of Energy, Office of High Energy and Nuclear Physics, under Grant Nos. DE-FG02-97-ER41042 and DE-FG02-97-ER41033, and by the U.S. Department of Energy, Office of Energy Research, under Contract No. W-7405-ENG-36.

[1] V. P. Alfimenkov, S. B. Borzakov, Vo Van Thuan, Yu. D. Mareev, L. B. Pikelner, A. S. Khrykin, and E. I. Sharapov, Nucl. Phys. **A398**, 93 (1983).
[2] E. G. Adelberger and W. C. Haxton, Annu. Rev. Nucl. Part. Sci. **35**, 501 (1988).
[3] B. Desplanques, J. F. Donoghue, and B. R. Holstein, Ann. Phys. (N.Y.) **124**, 449 (1989).
[4] J. D. Bowman, G. T. Garvey, Mikkel B. Johnson, and G. E. Mitchell, Annu. Rev. Nucl. Part. Sci. **43**, 829 (1993).
[5] C. M. Frankle, S. J. Seestrom, N. R. Roberson, Yu. P. Popov, and E. I. Sharapov, Phys. Part. Nuclei **24**, 401 (1993).
[6] V. V. Flambaum and G. F. Gribakin, Prog. Part. Nucl. Phys. **35**, 423 (1995).
[7] J. D. Bowman *et al.*, Phys. Rev. Lett. **65**, 1192 (1990).
[8] X. Zhu *et al.*, Phys. Rev. C **46**, 768 (1992).
[9] C. M. Frankle *et al.*, Phys. Rev. Lett. **67**, 564 (1991).
[10] C. M. Frankle *et al.*, Phys. Rev. C **46**, 778 (1992).
[11] S. L. Stephenson *et al.*, Phys. Rev. C **58**, 1236 (1998), the following paper.
[12] B. E. Crawford, Ph.D. thesis, Duke University, 1997.
[13] P. W. Lisowski, C. D. Bowman, G. J. Russell, and S. A. Wender, Nucl. Sci. Eng. **106**, 208 (1990).
[14] N. R. Roberson *et al.*, Nucl. Instrum. Methods Phys. Res. A **326**, 549 (1993).
[15] J. J. Szymanski *et al.*, Nucl. Instrum. Methods Phys. Res. A **340**, 564 (1994).
[16] S. I. Penttilä, J. D. Bowman, P. P. J. Delheij, C. M. Frankle, D. G. Haase, R. Mortensen, H. Postma, S. J. Seestrom, and Yi-Fen Yen, in *Time Reversal Invariance and Parity Violation in Neutron Resonances*, edited by C. R. Gould, J. D. Bowman, and Yu. P. Popov (World Scientific, Singapore, 1994), p. 198.
[17] S. I. Penttilä, J. D. Bowman, P. P. J. Delheij, C. M. Frankle, D. G. Haase, H. Postma, S. J. Seestrom, and Yi-Fen Yen, in *High Energy Spin Physics*, edited by K. J. Heller and S. L. Smith, AIP Conf. Proc. No. **343** (AIP, New York, 1995), p. 532.
[18] V. W. Yuan *et al.*, Phys. Rev. C **44**, 2187 (1991).
[19] J. D. Bowman, S. I. Penttilä, and W. B. Tippens, Nucl. Instrum. Methods Phys. Res. A **369**, 195 (1996).
[20] Yi-Fen Yen *et al.*, in *Time Reversal Invariance and Parity Violation in Neutron Resonances* (Ref. [16]), p. 210.
[21] C. M. Frankle, J. D. Bowman, S. J. Seestrom, N. R. Roberson, and E. I. Sharapov, in *Time Reversal Invariance and Parity Violation in Neutron Resonances* (Ref. [16]), p. 204.
[22] B. E. Crawford *et al.*, in *IV International Seminar on Interactions of Neutrons with Nuclei* (JINR, Dubna, 1997), p. 268.
[23] Y. Matsuda, Ph.D. thesis, Kyoto University, 1998.
[24] C. W. Reich and M. S. Moore, Phys. Rev. **111**, 929 (1958).
[25] Cross Section Evaluation Working Group, Report No. BNL-NCS-44945, 1997.
[26] S. F. Mughabghab, M. Divadeenam, and N. E. Holden, *Neutron Cross Sections* (Academic Press, New York, 1981), Vol. 1, Pt. A.
[27] J. E. Lynn, *The Theory of Neutron Resonance Reactions* (Clarendon Press, Oxford, 1968).
[28] Yi-Fen Yen, E. J. Pitcher, and J. D. Bowman (unpublished).
[29] M. C. Moxon and M. G. Sowerby, in Proceedings of the 1988 International Reactor Physics Conference, 1988 (unpublished), p. 281.
[30] D. K. Olsen, G. de Sausseure, R. B. Perez, F. C. Defilippo, R. W. Ingle, and H. Weaver, Nucl. Sci. Eng. **69**, 202 (1979).
[31] Yi-Fen Yen, J. D. Bowman, L. Y. Lowie, Y. Masuda, G. E. Mitchell, and S. I. Penttilä, Nucl. Instrum. Methods Phys. Res. A **397**, 365 (1997).
[32] L. M. Bollinger and G. E. Thomas, Phys. Rev. **171**, 1293 (1968).
[33] S. F. Mughabghab, M. Divadeenam, and N. E. Holden, *Neutron Cross Sections* (Academic Press, New York, 1988), Vol. 1, Pt. B.
[34] B. V. Carlson, M. S. Hussein, A. K. Kerman, and C.-Y. Lin, Phys. Rev. C **52**, 11 (1995).
[35] O. P. Sushkov and V. P. Flambaum, Pis'ma Zh. Eksp. Teor. Fiz. **32**, 377 (1980) [JETP Lett. **32**, 352 (1980)].
[36] V. E. Bunakov and V. P. Gudkov, Z. Phys. A **303**, 285 (1981).
[37] V. P. Alfimenkov, Usp. Fiz. Nauk **144**, 361 (1984) [Sov. Phys. Usp. **27**, 797 (1984)].
[38] J. R. Vanhoy, E. G. Bilpuch, J. F. Shriner, Jr., and G. E. Mitchell, Z. Phys. A **331**, 1 (1988).
[39] C. R. Gould, D. G. Haase, N. R. Roberson, H. Postma, and J. D. Bowman, Int. J. Mod. Phys. A **5**, 2181 (1990).
[40] J. D. Bowman, L. Y. Lowie, G. E. Mitchell, E. I. Sharapov, and Yi-Fen Yen, Phys. Rev. C **53**, 285 (1996).
[41] J. D. Bowman, L. Y. Lowie, and E. I. Sharapov, Phys. Part. Nuclei **27**, 398 (1996).
[42] F. Gunsing, K. Athanassopulos, F. Corvi, H. Postma, Yu. P. Popov, and E. I. Sharapov, Phys. Rev. C **56**, 1266 (1997).